ISSN 1063-7834, Physics of the Solid State, 2014, Vol. 56, No. 11, pp. 2160–2165. © Pleiades Publishing, Ltd., 2014.
Original Russian Text © F.F. Sizov, R.K. Savkina, A.B. Smirnov, R.S. Udovytska, V.P. Kladko, A.I. Gudymenko, N.V. Safryuk, O.S. Lytvyn, 2014, published in Fizika Tverdogo Tela, 2014, Vol. 56, No. 11, pp. 2091–2096.

SEMICONDUCTORS

Structuring Effect of Heteroepitaxial CdHgTe/CdZnTe Systems under Irradiation with Silver Ions

F. F. Sizov, R. K. Savkina, A. B. Smirnov, R. S. Udovytska, V. P. Kladko, A. I. Gudymenko, N. V. Safryuk, and O. S. Lytvyn

Lashkaryov Institute of Semiconductor Physics, National Academy of Sciences of Ukraine, pr. Nauki 41, Kyiv, 03028 Ukraine

e-mail: alex_tenet@isp.kiev.ua

Received March 5, 2014; in final form, June 2, 2014

Abstract—The characteristics of a damaged layer of p-$Cd_xHg_{1-x}Te$/CdZnTe ($x \sim 0.223$) heterostructures after implantation by 100-keV silver ions with the implantation dose $Q = 3.0 \times 10^{13}$ cm^{-2} have been obtained using X-ray diffraction, atomic force microscopy, and electron microscopy. It has been found that, as a result of the ion implantation and subsequent annealing (75°C), a uniform array of nanostructures is formed on the surface of Hg(Cd)Te/Zn(Cd)Te samples. The X-ray diffraction patterns of the structurized Hg(Cd)Te/Zn(Cd)Te sample indicate the formation of polycrystalline Hg(Cd)Te phases of cubic structure with a composition $x \sim 0.20$ and also oxide Ag_2O in the subsurface (<100 nm) region of the host material. The observed effects of transformation of the defect–impurity system and structuring of the surface of the heteroepitaxial film of the low-energy-gap semiconductor have been explained using a deformation model.

DOI: 10.1134/S1063783414110286

1. INTRODUCTION

Modern semiconductor technologies are essentially the art of "defect engineering" that makes it possible to precisely vary the properties of a semiconducting material with the lowest energy consumption [1]. So, a wide spectrum of topological features of a semiconductor surface can be developed by ion implantation [2]. For example, the implantation of ions of magnetic (or nonmagnetic) metals makes it possible to synthesize nanostructured layers exhibiting both diamagnetic and superparamagnetic or even ferromagnetic properties in a thin subsurface layer of an irradiated matrix [3]. A topical problem of ion implantation is the formation of composite structures of the "nanocrystalline inclusion–matrix" type [4].

In low-energy-gap mercury-containing semiconductors, among them are cadmium–mercury–tellurium (CMT) solid solutions, the energy transmitted during radiation treatment and consumed to control their impurity-defect structure is often excessive [5]. The substantial sensitivity of the semiconducting material to an external action is due to a low threshold of defect formation (the enthalpy of the Hg–Te bond formation $\Delta H_f = 0.33$ eV [6]) and a significant number of intrinsic electrically active defects in the initial state [7]. The electrophysical and photoelectric characteristics of the CMT solid solution are changed (up to the change in the conduction type) even under such low-energy action as the ultrasonic treatment [8]. During the ion implantation, the region of radiation damage of the CMT crystal structure is saturated with vacancies V_{Hg}, mercury interstitials, and anti-site tellurium Te_{Me}. In this case, the transformation of the defect system can be significant, so that the physical value of ion doping is negated even in the case of a low-energy regime of the process [5].

The aim of this work is to study the specific features of generation and removal of mechanical stresses in the doped layer and to perform the characterization of defects in subsurface regions of the heteroepitaxial Hg(Cd)Te/Zn(Cd)Te system using the substantially nonequilibrium method of silver implantation.

2. SAMPLE PREPARATION AND EXPERIMENTAL TECHNIQUE

We consider p-type semiconductor $Cd_xHg_{1-x}Te$/CdZnTe ($x \sim 0.223$) structures grown by liquid-phase epitaxy. The samples were irradiated by Ag^+ ions on the side of the CMT heterolayer on a Vezuvii-5 implanter. The implantation energy and dose were 100 keV and $Q = 3.0 \times 10^{13}$ cm^{-2}, respectively. After the implantation, the samples were held in the chamber at an excess argon pressure of 4 bar and at a temperature of 75°C for 5 h. The temperature conditions and the technique of heat treatment of the samples allowed us to avoid the oxidation of the damaged layer ("to observe" a surface charge) and to activate ion migration in the layer [9, 10].

The sample surface state before and after the implantation and also after performed annealings was

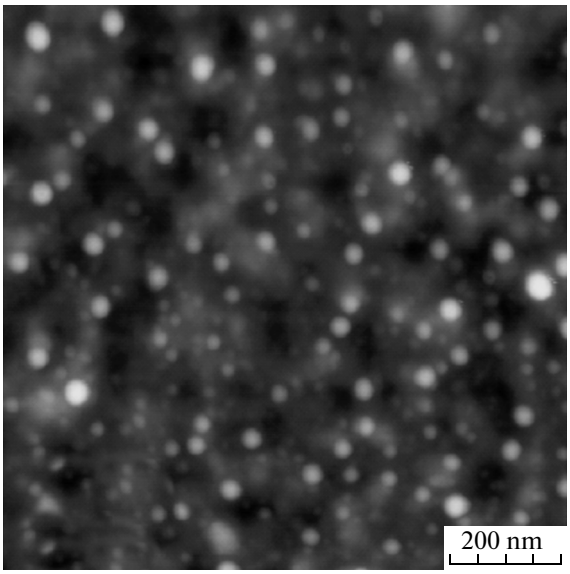

Fig. 1. AFM image of the surface of the Ag^+-implanted $Cd_xHg_{1-x}Te$/CdZnTe ($x \sim 0.223$) sample after annealing.

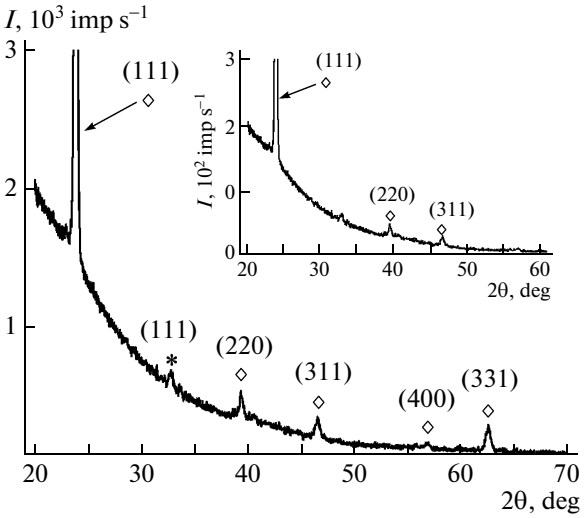

Fig. 2. Grazing incidence X-ray diffraction pattern of the $Cd_xHg_{1-x}Te$/CdZnTe ($x \sim 0.223$) heterostructure sample after implantation with Ag^+ ions. The X-ray radiation penetration depth is less than 200 nm at $\theta_{inc} = 1°$: (◇) $Cd_{0.20}Hg_{0.80}Te$ and (*) Ag_2O. The inset shows the X-ray diffraction pattern of the sample in the Bragg configuration.

controlled by atomic force microscopy (AFM, NanoScope IIIa Digital Instruments) and electron microscopy (Tescan Mira3 LMU).

An informative method of studying ion-implanted multilayer systems is X-ray diffraction [11]. An analysis of X-ray diffraction reflection curves allows one to characterize the sharpness of the heteroboundary, deformation, composition, and structural characteristics of epitaxial layers [12, 13]. The quantitative structural characterization of Hg(Cd)Te heterosystems is hampered by damages of different origins, which increases the relevance of X-ray diffraction methods and stimulates their improvement.

The structural changes in the surface of the Hg(Cd)Te solid solution were studied using the double- and three-crystal X-ray diffractometry [12]. The X-ray diffraction studies were performed on a Panalytical X-Pert PRO MRD (Almelo, The Netherlands) diffractometer using characteristic CuK_α radiation. The monochromatization of X-rays was carried out using a 4 × Ge(220) monochromator and a 2 × Ge(220) analyzer, which substantially increases the resolution of the apparatus and allows one to measure the relative change in the crystal lattice parameter accurate to $\Delta a/a = 10^{-5}$. The 17-μm-thick CMT epitaxial layer was considered as a bulk crystal with a damaged subsurface layer.

3. RESULTS AND DISCUSSION

The AFM image of a surface portion of a typical implanted CMT sample is shown in Fig. 1, which demonstrates the formation of an array of nanometer-size objects. The AFM topometry of the initial samples shows the existence of a network of quasi-pores with a depth of 3.5–10 nm and a diameter of 50–160 nm with 40- to 80-nm grains, which are closely packed in the surface plane. After the silver ion implantation, a uniform array of cone-like structures with a height from 5 to 25 nm and a base diameter from 13 to 35 nm is formed on the surface of the samples against the background of the small smearing of grain boundaries but with the initial porosity.

The simulation of the implantation process performed in [14] using the TRIM_2008 software package revealed that the introduced impurity is mainly localized in the subsurface region (~100 nm) of CMT. The ellipsometry data also indicate that, in the silver-implanted CdHgTe/CdZnTe samples, there is a damaged layer ~100 nm thick with anomalous values of the extinction coefficient and refractive index [14].

In this connection, the structural properties of the subsurface layer of the implanted CMT samples were studied grazing incidence X-ray diffraction. The incidence angle of the X-ray beam was chosen, so that to obtain information from a depth ~100 nm. The X-ray penetration depth was estimated by expression $2\theta_{inc}/\mu$, where μ is the linear coefficient of X-ray attenuation that is $\sim 1.5 \times 10^3$ cm^{-1} for CdTe (and also CdZnTe) at the X-ray radiation energy used in [15]. The values of θ_{inc} and the penetration depth are given in the subscription to Fig. 2.

The grazing incidence X-ray diffraction pattern (Fig. 2) indicates the formation of the polycrystalline

Results of X-ray diffractometry of a typical $Cd_xHg_{1-x}Te$/CdZnTe sample ($x \sim 0.223$)

Sample	Lattice parameter a, Å	FWHM, arcsec		
		ω–2θ scan	ω scan	ω scan, DCD*
Initial	6.4631	22.4	26.8	64.4
After the Ag^+ implantation	6.4659	20.5	48.4	68.0
After annealing	6.4637	26.8	51.3	73.0

* Double-crystal diffractometer.

phase of the cubic structure with composition $x = 0.2$ and lattice parameter $a = 6.4654$ Å (ICDD PDF 00-051-1122).[1] The X-ray diffraction pattern also contains a peak at the angle of 32.7°, which corresponds to the (111) reflection from Ag_2O (ICDD PDF 00-041-1104) with the lattice parameter $a = 4.7263$ Å. The high level of the background and smeared low-intense bands can demonstrate that the region under study has a disordered structure undergoing a phase transition [16–18]. According to the Scherrer relationship [19, 20], the coherent scattering domain size is 70 nm for the Ag_2O (111) peak and 200 nm for the CMT (111) peak. The inset in Fig. 2 shows the X-ray diffraction pattern of the sample in the Bragg configuration. The X-ray diffraction data for a typical $Cd_xHg_{1-x}Te$/CdZnTe ($x \sim 0.223$) sample obtained in the symmetric configuration are given in table. We determined the lattice parameter that is 6.4631 Å for the initial sample and indicates the anomalously low cadmium content in the solid solution ($x = 0.156$) that does not correspond to the content assumed. The Cd concentration was determined by the Vegard law [21]. At the same time, the energy-dispersion X-ray microanalysis of the initial sample surface (network with a step of 80 μm) and also the IR Fourier spectroscopy data indicate the correspondence of the composition of the semiconducting material heterolayer to the technological passport ($x \sim 0.223$). The differences of the composition and structural characteristics of the initial material are $\Delta x = -0.067$ ($x_0 = 0.223$) and $\Delta a = -0.0029$ Å ($a_0 = 6.4660$ Å), respectively.

The cause of the observed disagreement in Hg(Cd)Te system can be the crystal lattice compression due to high mercury vacancy concentration in the initial sample ($p \sim 10^{17}$ cm^{-3}). For example, it was stated in [22] that the Cd contents in the CMT solid solution determined by X-ray diffraction and energy-dispersion microanalysis differ by more than 10%. The difference is explained by the effect of the crystal lattice compression due to high mercury vacancy concentration (~10^{17}–10^{18} cm^{-3}). Similar action of point defects on the lattice parameter in SiGe solid solutions was also noted in [22].

[1] According to the International Centre for Diffraction Data (ICDD) Powder Diffraction Files (PDF).

Thus, the initial CMT material exhibits static damages with compression strains $\varepsilon_1 = (a_{CdHgTe} - a_0)/a_{CdHgTe} = -4.485 \times 10^{-4}$. The silver implantation of the samples shifts the diffraction maximum of (ω–2θ) curves toward lower angles. The CMT crystal lattice parameter increases with respect to the initial value (a_{CdHgTe}) by the value $\Delta a = 0.0028$ Å (table). The initially compressed CMT heterolayer is expanded. Actually, the deformation of the semiconducting material, as a result of implantation, recovers the deficit of parameter a and, along with this, recovers the sample stoichiometry. A subsequent annealing leads to a partial relaxation in the damaged CMT layer. The solid solution returns to the nonstoichiometric region and to stress-compressed state (table).

Figures 3a and 3b show the distribution maps of the diffuse scattering around site 111 in the reciprocal space for the sample of the $Cd_xHg_{1-x}Te$/CdZnTe ($x \sim 0.223$) heteroepitaxial structure before and after the silver ion implantation. The maps are a bonded set of scans perpendicularly (q_x) and parallel (q_z) to the diffraction vector. The observed distribution of the intensity along axis q_z indicates the existence in the initial material of a significant structural heterogeneity caused by the existence of microdefects of the vacancy ($q_z < 0$) and interstitial ($q_z > 0$) types (Fig. 3a). The formation of the significant halo in the central part of the map of the implanted sample (Fig. 3b) indicates the increase in the CMT film imperfection after the implantation performed.

In addition, we revealed significant increase in the intensity of diffuse scattering perpendicularly to the diffraction vector (q_x direction). The isodiffuse curves demonstrate the increase in the half-width of the ω scan (the last column of the table). Formally, it can mean the formation in the material of defect regions with local rotations of the crystal lattice (misorientation-type defects [23]).

However, the observed fact of precipitating the polycrystalline phase of CMT (Fig. 2) that has another composition ($x = 0.2$) than that of the matrix does not allow us to explain all the facts by the formation of defects. According to the conclusions from [23], the phase precipitation takes place upon the coherent isomorphic decomposition of the solid solutions; in this case, the thus-structurized material must have a

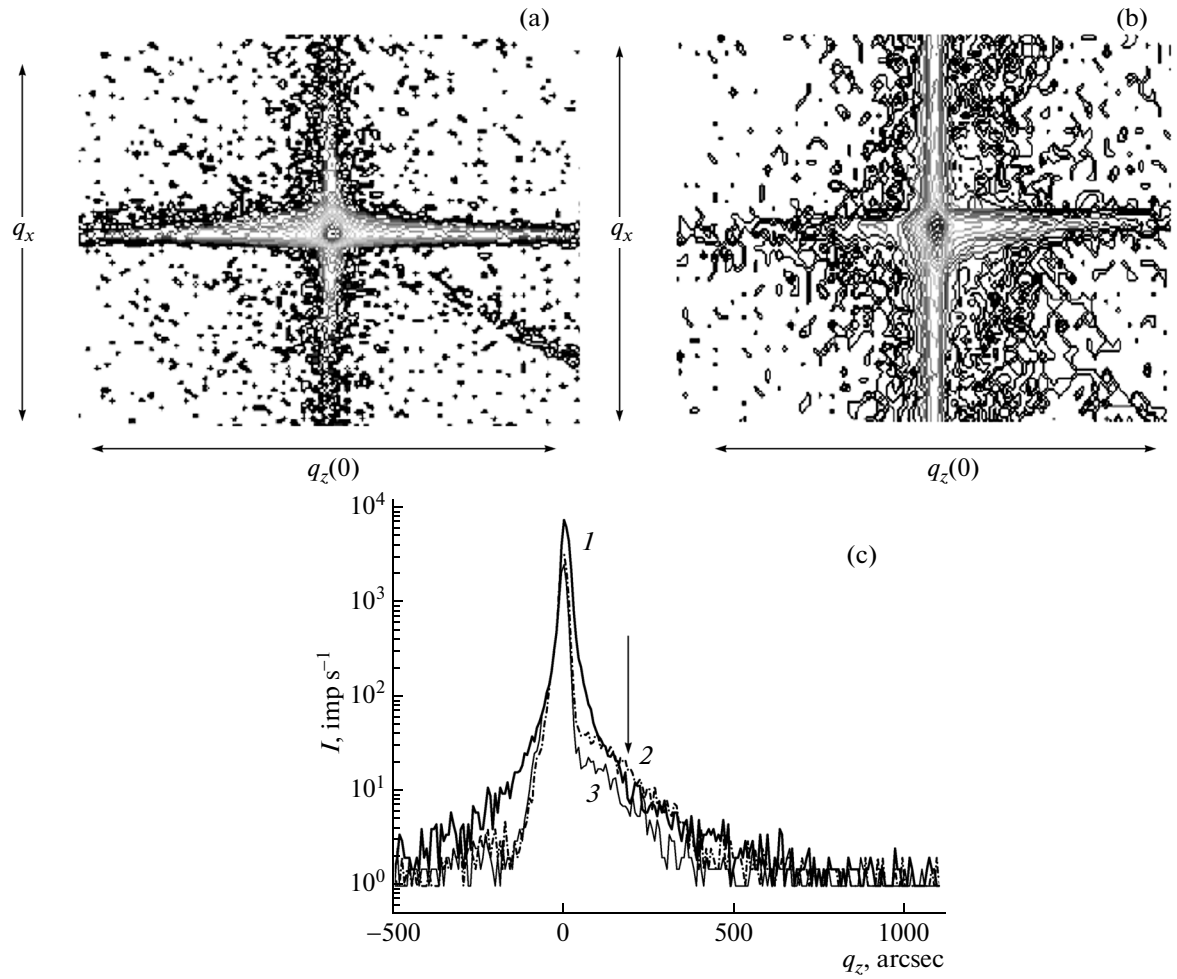

Fig. 3. Reciprocal space maps of the $Cd_xHg_{1-x}Te/CdZnTe$ ($x \sim 0.223$) heterostructure sample (a) before and (b) after Ag^+-ion implantation, obtained from the combined ω and (ω–2θ) scans using high-resolution modules. (c) Distribution of the intensity of diffuse scattering by the sample along the diffraction vector (q_z direction): (*1*) initial state of the sample, (*2*) after Ag^+-ion implantation, and (*3*) after annealing.

lamellar form with the dominant orientation in the direction perpendicular to the crystallographic equivalent directions [17]. The polycrystalline layer also increases the diffuse scattering region in the direction perpendicular to the diffraction vector (q_x direction) [24]. Subsequent annealing of the sample increases the half-width of the ω scans (table), i.e., the degree of imperfection/disordering of the subsurface layer increases.

Another feature of the implanted sample is the decrease in the background and the appearance of asymmetry in the q_z direction (Fig. 3b), which is demonstrated in the table by the decrease in the FWHM parameter of the (ω–2θ) scans. An analysis of the q_z section in Fig. 3b shows that the curve for the implanted sample is asymmetric.

The structural transformation of the region subjected to the implantation is thought to occur due to the formation of a state with excess energy in a thin layer of the material and can be explained in the framework of the theory of physicochemistry of the activated state of a solid surface [25]. An analysis of the initial sample surface indicates the substructural growth nonequilibrium of the Hg(Cd)Te system under study. The charge particle (ion) flow additionally distorts the target crystal lattice; in this case, its specific surface and the degree of disordering increase up to the formation of the damaged layer with the optical and electrical characteristics different than those observed for the matrix; the silver concentration in the damaged layer is $\sim 10^{19}$ cm^{-3} [14]. In other words, the enthalpy of the Hg(Cd)Te increases. The subsequent relaxation of the nonequilibrium state of the semiconducting material can pass via the heat release, the formation of defects in the crystal structure, the formation of new surface up to the excitation of solid-phase chemical reactions [25].

We assume that the deformation fields appearing upon implantation of the studied heterostructure are a determining factor of the observed transformation of its surface. The deformation accumulation is found to lead to the topological instability of the irradiated surface [26, 27]. The deformation sign is dependent on the ratio of ionic radii of the matrix atoms and introduced impurity [28]. As a result of the silver ion implantation of the CMT solid solution ($r^+_{Ag} = 1.71$ Å is comparable to $r^+_{Hg} = 1.76$ Å and $r^+_{Cd} = 1.71$ Å), the local volume and extension of the crystal lattice increase, which is confirmed by the X-ray diffraction data. The calculated mechanical stress is $\sigma_{max} = 2 \times 10^5$ Pa [14]. As a result, each of the local volumes (blocks) of the crystal undergoes an action of forces from the neighboring blocks, and their resulting force and its impulse will not be zero because of fluctuations. When the stress will be higher than the ultimate strength of CMT, the action of the forces can brings about the rotation of small crystalline blocks and the structuring of the material.

According to the existing concepts of Hg(Cd)Te, a dominant process of transformation of defects in this material is the diffusion, interaction, and recombination of mercury vacancies and interstitial sites: $Hg_i + V_{Hg} = Hg_{Hg}$. The extension regions formed upon silver implantation into CMT shift the reaction to the left [28], and the compression of deeper layers of the loosened epitaxial film prevent the mercury diffusion into the target depth.

The vacancy material obtained using the liquid-phase epitaxy technology demonstrates the shape asymmetry (Fig. 3c) because of deformation damage; the asymmetry indicates the preferential increase in the CMT crystal lattice parameter. The existence of the shoulder in the curve of diffraction reflection on the side of large angles (Fig. 3c) confirms the fact of accumulation of unrecombined intrinsic defects, which is also demonstrated by the conservation of the initial porosity in the CMT samples after both implantation and heat treatment.

Note that silver exhibits a high penetrating capacity and the tendency to form high-labile solid solutions in CMT [29]. We failed to clearly determine the chemical composition of the nanostructures formed at the surface of the implanted samples. At the same time, the X-ray diffraction data unambiguously indicate the formation of a new phase in the subsurface layer of CMT. The cause of the observed self-organization of nanoheteroepitaxial metal–oxide–semiconductor structures at the surface of the implanted film is the process of structural stabilization of the nonequilibrium of the activated state of the Hg(Cd)Te system, which is controlled by the processes of elastic interaction in simplest defect ensembles [25].

4. CONCLUSIONS

We considered the structuring of subsurface regions of the heteroepitaxial Hg(Cd)Te/Zn(Cd)Te system during low-energy irradiation with silver ions. It was found that, as a result of the ion implantation and subsequent annealing, a uniform array of nanostructures with a height from 5 to 25 nm and a base diameter from 13 to 35 nm is formed on the surface of the *p*-$Cd_xHg_{1-x}Te$/CdZnTe ($x \sim 0.223$) samples. The X-diffraction patterns of the structurized Hg(Cd)Te/Zn(Cd)Te sample show that the polycrystalline Hg(Cd)Te cubic phase with $x \sim 0.20$ and the metal oxide phase (Ag_2O) are formed in the subsurface (<100 nm) region of the host material.

The X-ray diffraction analysis revealed the difference in the composition and structural characteristics ($\Delta x = -0.067$ Å and $\Delta a = -0.0029$ Å for the initial "vacancy" material $Cd_xHg_{1-x}Te$ ($x \sim 0.223$); the difference is due to the deformation damage of the CMT crystal lattice by intrinsic point defects, namely, mercury vacancies.

The obtained results can be used to enhance the efficiency of semiconductor photoconverters and to increase the adhesion of specific coatings [30] deposited on the Hg(Cd)Te surface. The question about the silver oxidation and photoactivity of nanoheteroepitaxial metal–oxide–semiconductor structures remains open; the studies of the stability of this system in time are necessary too.

REFERENCES

1. N. A. Sobolev, Semiconductors **44** (1), 1 (2010).
2. J. B. Malherbe, in *Ion Beam Analysis of Surfaces and Interfaces of Condensed Matter Systems*, Ed. by P. Chakraborty (Nova Science, New York, 2003), p. 357.
3. X. Battle and A. Labarta, J. Phys. D: Appl. Phys. **35**, R15 (2002); M. Holdenried and H. Micklitz, Eur. Phys. J. **13**, 205 (2000).
4. A. Meldrum, R. Lopez, R. H. Magruder, L. A. Boatner, and C. W. White, in *Materials Science with Ion Beams* (Springer-Verlag, Berlin, 2010), pp. 255–285.
5. K. D. Mynbaev and V. I. Ivanov-Omskii, Semiconductors **40** (1), 1 (2006).
6. V. B. Lazarev, *Physicochemical Properties of Semiconductor Substances* (Nauka, Moscow, 1979) [in Russian].
7. *Mercury Cadmium Telluride Growth, Properties and Applications*, Ed. by P. Capper and J. Garland (Wiley, New York, 2011).
8. R. K. Savkina, A. B. Smirnov, and F. F. Sizov, Semicond. Sci. Technol. **22**, 97 (2007).
9. A. M. White, J. Phys. D: Appl. Phys. **14** (1), L1 (1981).
10. Y. Nemirovsky and E. J. Finkman, Electrochem. Soc. **126**, 768 (1979).
11. V. P. Kladko, L. I. Datsenko, J. Bak-Misiuk, S. I. Olikhovskii, V. F. Machulin, I. V. Prokopenko, V. B. Molodkin, and Z. V. Maksimenko, J. Phys. D: Appl. Phys. **34**, A87 (2001).

12. A. N. Efanov and V. P. Kladko, Metallofiz. Noveishie Tekhnol. **28** (2), 227 (2006).
13. V. B. Molodkin, S. I. Olikhovskii, E. G. Len, E. N. Kislovskii, V. P. Kladko, O. V. Reshetnyk, T. P. Vladimirova, and B. V. Sheludchenko, Phys. Status Solidi A **206**, 1761 (2009).
14. A. B. Smirnov, O. S. Lytvyn, V. O. Morozhenko, R. K. Savkina, M. I. Smoliy, R. S. Udovytska, and F. F. Sizov, Ukr. J. Phys. **58** (9), 872 (2013).
15. A. Rogalski, Prog. Quantum Electron. **36**, 342 (2012).
16. H. P. Klug and L. E. Alexander, *X-Ray Diffraction Procedures for Polycrystalline Amorphous Materials*, 2nd ed. (Wiley, New York, 1974), p. 791.
17. M. A. Krivoglaz, *Diffuse Scattering of X-Rays and Neutrons by Fluctuation Inhomogeneities in Imperfect Crystals* (Naukova Dumka, Kiev, 1984) [in Russian].
18. J.-M. Lehn, *Supramolecular Chemistry* (Wiley, New York, 1995; Nauka, Novosibirsk, 1998).
19. B. D. Cullity, *Elements of X-Ray Diffraction* (Addision-Wesley, New York, 1978).
20. Landolt–Börnstein: *Numerical Data and Functional Relationships in Science and Technology*, Ed. by K. H. Hel-lwege (Springer-Verlag, Berlin, 1982), Vol. 17, p. 227.
21. I. Utke, L. Parthier, and M. Shenk, J. Cryst. Growth **123**, 269 (1992).
22. S. N. Yakunin and N. N. Dremova, JETP Lett. **87** (9), 494 (2008).
23. A. I. Gusev, *Nanocrystalline Materials: Methods of Preparation and Properties* (Ural Branch of the Russian Academy of Sciences, Yekaterinburg, 1998) [in Russian].
24. V. P. Kladko, A. V. Kuchuk, P. M. Lytvyn, O. M. Yefanov, N. V. Safriuk, A. E. Belyaev, Yu. I. Mazur, E. A. DeCuir, Jr., M. E. Ware, and G. J. Salamo, Nanoscale Res. Lett. **7**, 289 (2012).
25. K. Meyer, *Physikalisch-chemische Kristallographie* (Grundstoffindustrie, Leipzig, 1968; Metallurgiya, Moscow, 1972) [in German and in Russian].
26. T. Egami and Y. Waseda, J. Non-Cryst. Solids **64**, 113 (1984).
27. L. S. Palatnik, P. G. Cheremskoi, and M. Ya. Fuks, *Pores in Films* (Energoizdat, Moscow, 1982) [in Russian].
28. H. Ebe, M. Tanaka, and Y. Miyamoto, J. Electron. Mater. **28** (6), 854 (1999).
29. M. I. Ibragimova, V. Yu. Petukhov, and I. B. Khaibullin, Semiconductors **27** (4), 311 (1993).
30. N. I. Klyui, V. B. Lozinskii, A. N. Luk'yanov, V. A. Morozhenko, R. K. Savkina, F. F. Sizov, A. B. Smirnov, and V. A. Deriglazov, Tech. Phys. **57** (8), 1121 (2012).

Translated by Yu. Ryzhkov